of the antibiotic alone to cause sustained suppression of lethality in this model is likely due to host inflammatory response to endotoxin released from bacteria killed by antibiotic (*20*); indeed, administration of antibiotic dramatically decreased blood bacterial counts, but plasma endotoxin level concomitantly increased in these animals (Fig. 3). This model of intraperitoneal infection may thus be representative of the clinical situation for human sepsis (*2*).

We have developed a potent endotoxin antagonist E5531 by organic synthesis. In vitro studies showed E5531 to be a pure and specific LPS antagonist, while in vivo experiments demonstrated that E5531 protected BCG-primed mice from lethality induced by LPS and also death caused by viable *E. coli* infection. That these remarkable protective effects have been extended to humans (*21*) suggests that E5531 may be clinically useful in the treatment of Gram-negative sepsis and septic shock.

REFERENCES AND NOTES

1. R. C. Bone, *Chest* **100**, 802 (1991); J. E. Parrillo, *N. Eng. J. Med.* **328**, 1471 (1993).
2. S. Endo *et al.*, *Cir. Shock* **38**, 264 (1992); H. A. Crosby, J. F. Bion, C. W. Penn, T. S. J. Elliott, *J. Med. Microbiol.* **40**, 23 (1994); A. S. M. Dofferhoff *et al.*, *Scand. J. Infect. Dis.* **23**, 745 (1991); J. M. Prins, S. J. H. van Deventer, E. J. Kuijper, P. Speelman, *Antimicrob. Agents Chemother.* **38**, 1211 (1994).
3. C. Galanos *et al.*, *Eur. J. Biochem.* **148**, 1 (1985).
4. A. Billiau and F. Vandekerckhove, *Eur. J. Clin. Invest.* **21**, 559 (1991); M. P. Glauser, D. Heumann, J. D. Baumgartner, J. Cohen, *J. Clin. Infect. Dis.* **18** (suppl. 2), S205 (1994).
5. C. R. B. Welbourn and Y. Young, *Br. J. Surg.* **79**, 998 (1992); R. C. Bone, *Clin. Microbiol. Rev.* **6**, 57 (1993).
6. B. L. Ray, G. Painter, C. R. H. Raetz, *J. Biol. Chem.* **259**, 4852 (1984); C. E. Bulawa and C. R. H. Raetz, *ibid.*, p. 4846.
7. R. L. Danner, K. A. Joiner, J. E. Parrillo, *J. Clin. Invest.* **80**, 605 (1987).
8. R. A. Proctor, J. A. Will, K. E. Burhop, C. R. H. Raetz, *Infect. Immun.* **52**, 905 (1986); D. T. Golenbock, J. A. Will, C. R. H. Raetz, R. A. Proctor, *ibid.* **55**, 2471 (1987).
9. R. L. Danner, A. L. Van Dervort, M. E. Doerfler, P. Stuetz, J. E. Parrillo, *Pharm. Res.* **7**, 260 (1990).
10. J. H. Krauss, U. Seydel, J. Weckesser, H. Mayer, *Eur. J. Biochem.* **180**, 519 (1989).
11. H. Loppnow *et al.*, *Infect. Immun.* **58**, 3743 (1990); N. Qureshi, J. P. Honovich, H. Hara, R. J. Cotter, K. Takayama, *J. Biol. Chem.* **263**, 5502 (1988); K. Takayama, N. Qureshi, B. Beutler, T. N. Kirkland, *Infect. Immun.* **57**, 1336 (1989).
12. M. Imoto, H. Yoshimura, N. Sakaguchi, S. Kusumoto, T. Shiba, *Tetrahedron Lett.* **26**, 1545 (1985).
13. W. J. Christ *et al.*, U.S. Patent Application 935050 (1992).
14. W. J. Christ *et al.*, *J. Am. Chem. Soc.* **116**, 3637 (1994).
15. T. Kawata *et al.*, *Abstr. 32nd Intersci. Conf. Antimicrob. Agents Chemother.* **1992**, 1360 (1992).
16. B. K. Felber and G. Pavlakis, *Science* **239**, 184 (1988).
17. W. J. Christ *et al.*, in preparation.
18. D. Rossignol *et al.*, *Abstr. 32nd Intersci. Conf. Antimicrob. Agents Chemother.* **1992**, 1361 (1992).
19. S. N. Vogel, R. N. Moore, J. D. Sipe, D. L. Rosenstreich, *J. Immunol.* **124**, 2004 (1980).
20. O. Røkke, A. Revhaug, B. Østerud, K. E. Gierscksky, *Prog. Clin. Biol. Res.* **272**, 247 (1988).
21. In phase I clinical trials with healthy volunteers, E5531 was found to be devoid of LPS-like agonistic or toxic side effects. When co-administered at 100 or 1000 μg per subject with a low-dose endotoxin challenge (4 ng of LPS per kilogram of body weight), E5531 demonstrated dose-dependent decreases in the incidence and severity of cytokine release, fever, tachycardia, hypotension, and other LPS-induced signs and symptoms; see E. Bunnell *et al.*, paper presented at the 24th Educational and Scientific Symposium, Society for Critical Care Medicine, San Francisco, January 1995.
22. D. J. Stuehr and C. J. Nathan, *J. Exp. Med.* **169**, 1543 (1989); S. C. Wang *et al.*, *Surgery* **116**, 339 (1994).

14 September 1994; accepted 10 January 1995

Stretching of a Single Tethered Polymer in a Uniform Flow

Thomas T. Perkins, Douglas E. Smith, Ronald G. Larson, Steven Chu*

The stretching of single, tethered DNA molecules by a flow was directly visualized with fluorescence microscopy. Molecules ranging in length (L) from 22 to 84 micrometers were held stationary against the flow by the optical trapping of a latex microsphere attached to one end. The fractional extension x/L is a universal function of $\eta v L^{0.54 \pm 0.05}$, where η and v are the viscosity and velocity of the flow, respectively. This relation shows that the DNA is not "free-draining" (that is, hydrodynamic coupling within the chain is not negligible) even near full extension (~80 percent). This function has the same form over a long range as the fractional extension versus force applied at the ends of a worm-like chain. For small deformations (<30 percent of full extension), the extension increases with velocity as $x \sim v^{0.70 \pm 0.08}$. The relative size of fluctuations in extension decreases as $\sigma_x/x \cong 0.42 \exp(-4.9\, x/L)$. Video images of the fluctuating chain have a cone-like envelope and show a sharp increase in intensity at the free end.

The deformation of polymers in hydrodynamic flows is a fundamental and still incompletely resolved problem in polymer physics (*1*, *2*). The major difficulty in theoretical descriptions of polymer chain dynamics is the hydrodynamic coupling within the chain—the motion of one part of the chain perturbs the surrounding flow and modifies the hydrodynamic force exerted on another part. Here we present results of the stretching of single, tethered DNA molecules in a uniform fluid flow.

Direct observation and controlled deformation of individual DNA molecules gives insights into the previously inaccessible regime of single polymer dynamics (*3*–*6*). Earlier, we observed the relaxation of stretched DNA molecules in dilute and concentrated polymer solutions, using optical tweezers (*7*) and fluorescence microscopy (*3*, *5*, *6*). The present experiment addresses the balance of forces between hydrodynamic drag on a deformed polymer and its entropic elasticity. In earlier work, Smith *et al.* measured the extension of single DNA molecules stretched by a force applied at the ends (*4*). They attached one end to a surface and exerted a combination of magnetic and hydrodynamic forces on a magnetic microsphere at the other end (*4*). Because the forces exerted on the microsphere were larger than the hydrodynamic drag due to the DNA, Smith *et al.* measured primarily the elastic force, a static property of a polymer in solution. Theoretical calculations (*8*, *9*) show quantitative agreement between the elasticity data and the force law for a worm-like chain and give an approximate formula (*8*) of

$$\frac{FA}{k_B T} = \frac{1}{4}\left(1 - \frac{x}{L}\right)^{-2} - \frac{1}{4} + \frac{x}{L} \qquad (1)$$

where F is the force applied across the ends, A is the persistence length, x is the extension, L is the length of the polymer, and $k_B T$ is the thermal energy.

We made our measurements by optically trapping a microsphere attached to one end of a DNA molecule while the other end remained free. In this way we were able to investigate the hydrodynamic interaction between the polymer and the fluid. The chain was positioned away from any surface, and we elongated it in a uniform (nonshearing) flow by translating the fluid past the trapped, stationary microsphere (Fig. 1A). By determining the scaling properties of the system as a function of polymer length and solvent viscosity, we investigated the effects of hydrodynamic coupling. As Zimm showed (*10*), the hydrodynamic coupling within a polymer near equilibrium causes, in the simplest case, the total hydrodynamic drag to scale as $F_{drag} \sim L^{0.5}$. If hydrodynamic cou-

T. T. Perkins, D. E. Smith, S. Chu, Department of Physics, Stanford University, Stanford, CA 94305, USA.
R. G. Larson, AT&T Bell Laboratories, Murray Hill, NJ 07974, USA.
*To whom correspondence should be addressed.

pling is negligible, the chain is said to be "free-draining" and the hydrodynamic drag would be $F_{drag} \sim L$. It is often assumed that a polymer would become free-draining in the limit of large extensions. For example, de Gennes modeled the hydrodynamic shape of a polymer in an elongational flow as a cylinder into which the flow field penetrated on a finite length scale, making the chain free-draining in the limit of large extensions (*11*).

In our experiment, we used a broad range of fluid velocities (v) and two different viscosities (η), 0.95 and 2.9 cP (centipoise) (Fig. 1B). When the extension is plotted versus the product of the viscosity and the velocity, the data for both viscosities overlap, suggesting that the hydrodynamic drag on the chain is a function of ηv (*12*). Furthermore, this overlap of the data for a 0.3- and a 1.0-μm sphere shows that perturbation on the hydrodynamic drag due to the bead is small (*13*).

Remarkably, the functional dependence of the extension versus flow velocity is the same as the extension versus force data of Smith *et al.* (*4*) for fractional extensions of ~20 to 90% (Fig. 1C). This correspondence is unexpected and nontrivial because the nature of the force applied to the chain in the two cases is quite different. In our case, the applied force was zero at the free end; in contrast, in the experiment of Smith *et al.* the dominant force was applied to the end of the chain by means of the attached microsphere. Nevertheless, this functional correspondence allowed us to determine an asymptotic length of partially stretched chains by fitting our data to the force law given by Eq. 1. This fitted, asymptotic length is robust and changed by only 3% as the last data point was decreased from 183 to 12 cP μm s^{-1}. However, our data at the largest extensions (>90%) are slightly higher than the values predicted by Eq. 1 (*14*).

To look for scaling properties of the system, we measured the extension as a function of velocity (1 to 80 μm s^{-1}) and chain length (22 to 84 μm), using a 0.3-μm sphere to minimize the disturbance to the fluid flow (Fig. 2A). These sets of data collapsed onto a single curve when the fractional extension (x/L) was plotted versus vL^{α} with $\alpha = 0.54 \pm 0.05$ (Fig. 2B); this result shows that the fractional extension is a function of $\eta v L^{0.54}$ when combined with the functional dependence shown in Fig. 1B. When x/L is plotted versus vL, as suggested by the free-draining model, the data for molecules of different lengths do not collapse onto a universal curve, even for extensions as large as $x/L \sim 0.80$.

This universal functional form of the extension demonstrates that the DNA molecule is not free-draining. For a free-draining chain, the tension would increase as $F(s) = \gamma v s$, where γ is a constant drag coefficient

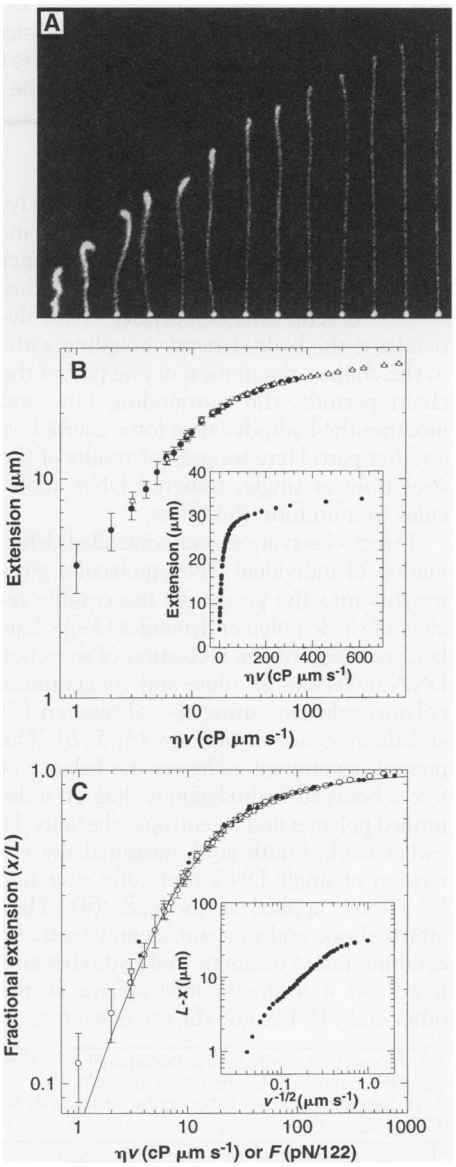

Fig. 1. (**A**) Images of a fluorescently labeled, 64.6-μm-long DNA molecule tethered at one end to a 0.3-μm latex sphere and deformed by constant fluid flows of v = 1, 2, 3, 4, 5, 7, 10, 12, 15, 20, 30, 40, and 50 μm s^{-1} with a viscosity of η = 0.95 cP. The microsphere was held stationary against the applied flow with optical tweezers and suspended 12 μm below the surface of the cover slip (*26*). To generate a flow around the trapped, stationary microsphere, the microscope stage was moved at a constant velocity of 1 to 200 μm s^{-1} with a feedback-controlled motor (*27*). The fractional extensions are (x/L) = 15, 22, 31, 38, 42, 49, 60, 63, 67, 72, 78, 81, and 83%, respectively. (**B**) A log-log plot of the extension versus the product of viscosity (η) and velocity (v) for a 34.6-μm-long DNA molecule (*28*). To minimize the fluid disturbance by the microsphere, we used a 0.3-μm sphere and a viscosity of η = 0.95 cP (filled circles). To generate larger hydrodynamic forces, we increased the viscosity to η = 2.9 cP, and to trap at these higher forces, we used a 1.0-μm-diameter sphere (open triangles). The superposition of both data sets confirms that the extension is a function of ηv. (Inset) All of the data plotted with linear scales. (**C**) Comparison of the extension versus flow velocity data (open circles) to the predicted form of the force versus extension law for a worm-like chain with a force applied at the ends (solid line) and the elasticity data of Smith *et al.* (*4*) (filled circles). The elasticity data (in piconewtons) was multiplied by 122 to overlay our experimental data. (Inset) Plot of $(L - x)$ versus $v^{-1/2}$. This plot shows the deviation of the experimental data from the functional form of the dominant term of Eq. 1 at large extensions $[A/(1 - x/L)^{-2}]$. Within the dumbbell model, the linear portion of the plot shows the independence of hydrodynamic drag with respect to conformation. The first four data points (highest ηv) deviate from the linear behavior and were not used in determining an asymptotic length.

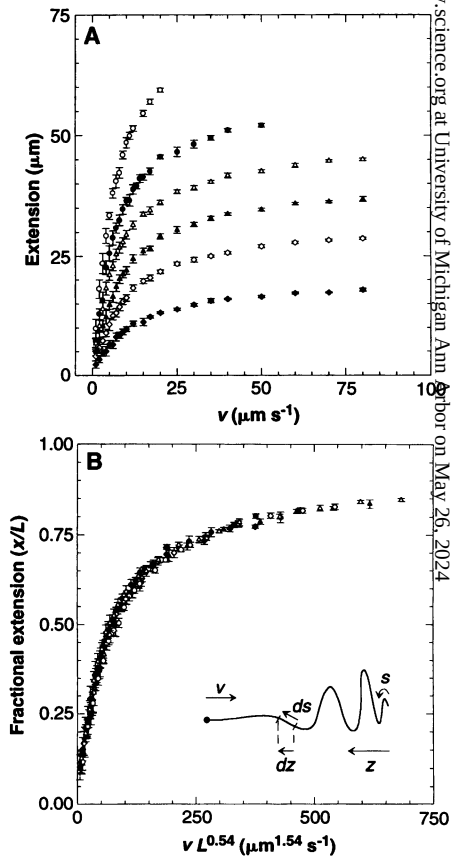

Fig. 2. (**A**) Plots of the extension versus applied flow velocity for DNA molecules of lengths 22.4, 34.8, 44.0, 53.1, 63.6, and 83.8 μm attached to a 0.3-μm sphere with a viscosity of η = 0.95 cP. (**B**) The fractional extension (x/L) plotted versus $vL^{0.54}$ collapsed the data to a universal curve. (Inset) Diagram used in the computation of the chain deformation (where s is the distance along the contour and z is the projection of s in the $-v$ direction).

per unit length and s is position along the chain contour from the free end (Fig. 2B, inset). The tension at one segment of the chain is due to the hydrodynamic drag of the downstream portion of the chain. The corresponding projected distance (z) antiparallel to the flow direction can be computed by integrating the local, coarse-grained stretching of the chain,

$$dz/ds = f^{-1}(FA/k_BT) \quad (2)$$

where f^{-1} is the inverse of a force function of the form $FA/k_BT = f(x/L)$. The total deformation is given by

$$x = \int_{s=0}^{L} \frac{dz}{ds}\,ds = \int_{s=0}^{L} f^{-1}\left(\frac{FA}{k_BT}\right)ds \quad (3)$$

Numerical integration of this expression with the force function given by Eq. 1 shows that x/L for a free-draining polymer is a universal function of $\eta\nu L$, in disagreement with the observed dependence (*15*). This analysis shows that the DNA, within the size range investigated, is not free-draining, despite being extended to almost its full contour length (~80%).

A chain that is not free-draining interacts with and modifies the surrounding fluid flow differently from a free-draining chain. DNA undergoing electrophoresis in solution is thought to be free-draining as a result of counterion flow because it does not separate by molecular weight (*16*). Our measurements highlight the difference between electric and hydrodynamic forces on DNA. Similar single-molecule experiments could test this assumption that DNA driven by electric fields is free-draining. Further, turbulent drag reduction in dilute polymer solution is also caused by the interaction of extended polymers with the surrounding flow (*1*). Our results suggest that this interaction is different from what was previously believed and thus may aid in understanding this effect.

On an empirical level, our data show that a dumbbell model (with one bead held fixed, the other bead free, and a spring obeying the force law of Eq. 1) may be used to predict the steady-state extension of the chain in a uniform flow. The flow extends the chain as if a force proportional to $\eta\nu L^{0.54}$ were applied at its end by means of a fictitious bead. The fictitious bead's radius (r_{eff}), and thus the chain's hydrodynamic drag, would be constant for a given chain length and would scale as $L^{0.54}$. As ν goes to 0, the size of the fictitious bead should scale as the radius of gyration (R_g) because the coil is only slightly deformed. Such independence of hydrodynamic drag with respect to extension is consistent with the calculations of Larson and Magda for extensional flows (*17*). Our measurements give r_{eff} = 0.6 μm for a 34.6-μm chain (*18*).

Although a dumbbell model describes the steady-state extension, it should only be valid for dynamic processes slower than the slowest relaxation time of the polymer (*1*, *19*). For example, the rate of relaxation predicted by this model ($dx/dt = -F/6\pi\eta r_{eff}$) in conjunction with the measured force law (Eq. 1) does not agree with the measured relaxation of tethered DNA molecules (*6*, *20*).

Fluctuations of the chain conformation are an important part of polymer dynamics. These fluctuations are due to Brownian motion and, in a flow, may also be driven by a variation in the hydrodynamic drag as the chain conformation changes. Present theories do not consider this latter type of variation in the hydrodynamic drag. To characterize the observed fluctuations, we computed the standard deviation (σ_x) in extension x (Fig. 3). The relative sizes for the fluctuations were well described by $\sigma_x/x \cong$

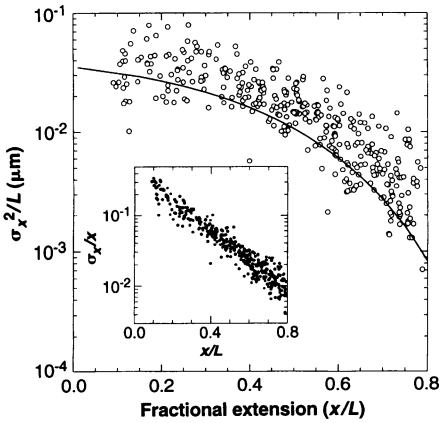

Fig. 3. Fluctuations, measured by the standard deviation (σ_x) about the mean extension, are compared to a dumbbell model prediction of thermally driven fluctuations in the end-to-end distance. Standard deviations corresponding to less than 2 pixels were excluded, which limited the fractional extension to less than 80%. (Inset) Log-linear plot of the relative size of fluctuations in extension versus fractional extension.

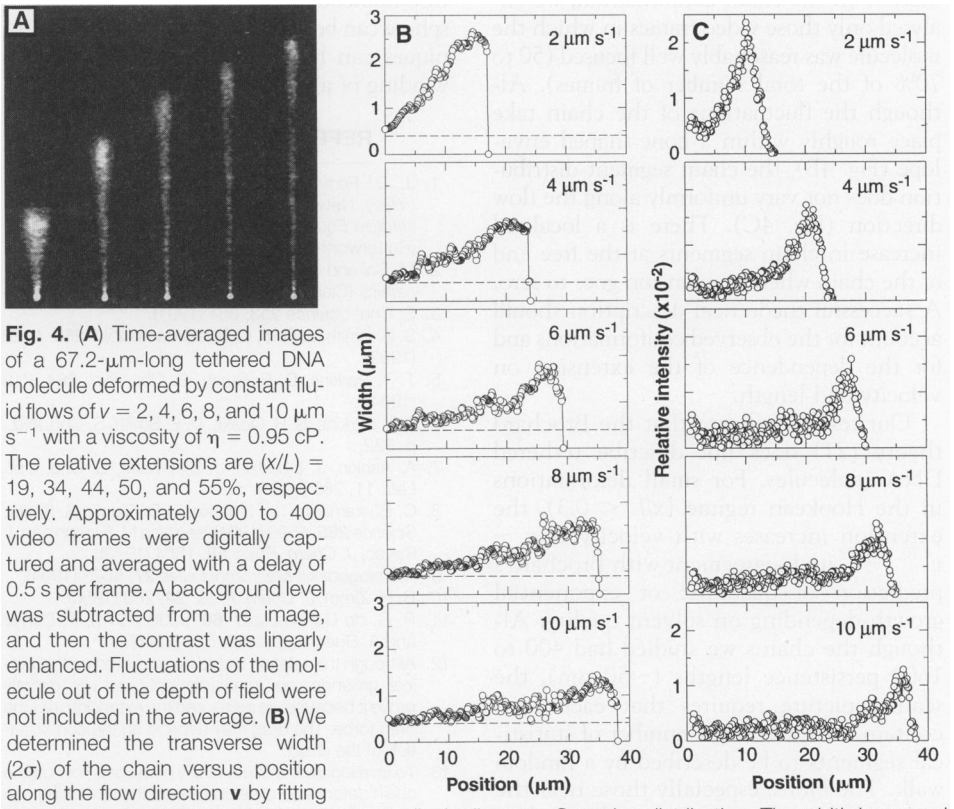

Fig. 4. (**A**) Time-averaged images of a 67.2-μm-long tethered DNA molecule deformed by constant fluid flows of v = 2, 4, 6, 8, and 10 μm s^{-1} with a viscosity of η = 0.95 cP. The relative extensions are (x/L) = 19, 34, 44, 50, and 55%, respectively. Approximately 300 to 400 video frames were digitally captured and averaged with a delay of 0.5 s per frame. A background level was subtracted from the image, and then the contrast was linearly enhanced. Fluctuations of the molecule out of the depth of field were not included in the average. (**B**) We determined the transverse width (2σ) of the chain versus position along the flow direction **v** by fitting the intensity distribution along each perpendicular line to a Gaussian distribution. The width increased approximately linearly along the chain. For comparison, the dashed line at 0.40 μm is the measured image width (2σ) of a highly extended DNA molecule (x/L = 0.91) stretched between two optical traps under the same imaging conditions. To reduce high-frequency noise for the purpose of fitting, we smoothed the images by convoluting each pixel with a two-dimensional Gaussian distribution (σ ≅ 0.13 μm). (**C**) We obtained normalized intensity profiles along the flow direction (**v**) for each of the images by summing the total intensity along each digital line perpendicular to **v**. These plots show the appearance, on average, of a ball of excess chain segments at the free end of the chain and the progressive decrease in size of the ball as the flow velocity is increased and the chain extends. The zero position is the location of the tether point, and the values associated with a small, fixed spot in the images were removed from the analysis. The data were normalized so that the area under each curve is equal to 1.

0.42 exp(−4.9 x/L). This decrease in fluctuations at higher extensions is caused by the nonlinear elasticity. As the spring stiffens, the fluctuations decrease. Within the dumbbell model, the fluctuations in extension can be modeled as thermal fluctuations of a fictitious bead in the potential well resulting from the balance between the elastic (Eq. 1) and the hydrodynamic forces. This calculation gives

$$\frac{\sigma_x^2}{L} = \frac{2A}{(1 - x/L)^{-3} + 2} \quad (4)$$

which qualitatively has the correct dependence and gives a value only 35% smaller in magnitude than the experimental data.

Direct visualization of the chain conformation gives us further insight into the deformation problem. Because the chain is uniformly labeled with dye molecules and the imaging system has linear gain, the chain segment distribution may be inferred from intensity measurements from instantaneous images (Fig. 1A) and time-averaged images (Fig. 4A). The images are a two-dimensional projection of an object fluctuating in three dimensions. To extract information on the chain conformation, we analyzed only those video frames in which the molecule was reasonably well focused (50 to 70% of the total number of frames). Although the fluctuations of the chain take place roughly within a cone-shaped envelope (Fig. 4B), the chain segment distribution does not vary uniformly along the flow direction (Fig. 4C). There is a localized increase in chain segments at the free end of the chain where the tension goes to zero. A successful theoretical description should account for the observed conformations and for the dependence of the extension on velocity and length.

Our results indicate that the Brochard theory (*21*) does not describe tethered DNA molecules. For small deformations in the Hookean regime ($x/L < 0.3$), the extension increases with velocity as $x \sim v^{0.70 \pm 0.08}$, in disagreement with Brochard's prediction of quadratic or exponential growth depending on solvent quality. Although the chains we studied had 400 to 1600 persistence lengths (~50 nm), the scaling picture requires that each blob contain a large enough number of statistical segments to be described by a random walk. The blobs, especially those near the microsphere, may not be in the scaling regime and may not entirely exclude the fluid flow.

Zimm, motivated by our measurements, modeled the stretching of a tethered polymer near equilibrium using a chain composed of multiple beads and Hookean springs (*22*). He replaced the force on each bead (F_{bead}) by the average over all beads and then computed the Oseen tensor using the Kirkwood-Riseman approximation (*2*, *23*). This leads to $F_{bead} \sim \eta v/L^{1/2}$ and, by summing the tension along chain, the fractional end-to-end extension of the polymer $R/L \sim \eta v L^{1/2}$, close to our experimental result of $x/L \sim (\eta v L^{0.54})^{0.7}$ for $x/L < 0.30$. As v goes to 0, the scaling of x with v may have an exponent that is smaller than unity because x is constrained to approach a constant, R_g, at zero velocity rather than zero while R is not so constrained. Although in this model each bead experiences the same force, it is the hydrodynamic coupling within the chain that leads to the rescaling of F_{bead} and thus the observed functional dependence.

For an investigation of the behavior far from equilibrium, a detailed comparison between theory and experiment can be made with numerical simulations by including Brownian motion and the worm-like–chain force law and by recalculating the hydrodynamic coupling between the beads at each extension (*24*). In future studies, it is expected that these measurements will be extended to longer molecules and to more complex flows involving velocity gradients. Also, the instantaneous force on the trapped microsphere can be measured (*25*), and these techniques can be applied to the dynamic unwinding of a polymer from a coil (*21*).

REFERENCES AND NOTES

1. J. D. Ferry, *Viscoelastic Properties of Polymers* (Wiley, New York, ed. 3, 1980); R. G. Larson, *Constitutive Equations for Polymer Melts and Solutions* (Butterworths, Boston, 1988).
2. M. Doi and S. Edwards, *The Theory of Polymer Dynamics* (Clarendon, Oxford, 1986).
3. S. Chu, *Science* **253**, 861 (1991).
4. S. B. Smith, L. Finzi, C. Bustamante, *ibid.* **258**, 1122 (1992).
5. T. T. Perkins, D. E. Smith, S. Chu, *ibid.* **264**, 819 (1994).
6. T. T. Perkins, S. R. Quake, D. E. Smith, S. Chu, *ibid.*, p. 822.
7. A. Ashkin, J. Dziedzic, J. Bjorkholm, S. Chu, *Opt. Lett.* **11**, 288 (1986).
8. C. Bustamante, J. F. Marko, E. D. Siggia, S. Smith, *Science* **265**, 1599 (1994); see also M. Fixman and J. Kovac, *J. Chem. Phys.* **58**, 1564 (1973).
9. A. Vologodskii, *Macromolecules* **27**, 5623 (1994).
10. B. H. Zimm, *J. Chem. Phys.* **24**, 269 (1956).
11. P. G. de Gennes, *ibid.* **60**, 5030 (1974); P. Debye and A. Bueche, *ibid.* **16**, 573 (1948).
12. Although this relation would be expected on theoretical grounds, our measurements do not directly prove it because we measured the extension, not the drag force. The drag may depend on the conformation of the chain.
13. To investigate the effect of the perturbed flow on the chain deformation, we compared the stretching of a chain of the same length attached to both bead sizes. The measured extension was the same for both bead diameters at velocities greater than 1 to 2 μm s^{-1}, indicating that the 0.3-μm bead was, at most, a small perturbation on the fluid flow over the range of velocities studied (1 to 200 μm s^{-1}).
14. Similar behavior was found in the experimental data of Smith *et al.* (*4*), and it was suggested that this might be the result of deformation of the DNA helix beyond the limit of entropic elasticity. By exerting even stronger forces with a meniscus (~500 pN), Bensimon *et al.* have observed stretching of DNA to approximately twice its crystallographic length [A. Bensimon *et al.*, *Science* **265**, 2096 (1994); D. Bensimon *et al.*, in preparation].
15. The observed universal functional dependence of x/L on $vL^{1/2}$ can be obtained in our calculation if one assumes that the tension in the chain varies as $F(s) = \beta v s^{1/2}$, where β is a constant. To interpret this as a position-dependent friction coefficient per unit length γ(*s*) and velocity field *v*(*s*), one could then write

$$F(s) = \int_{s=0}^{L} \gamma(s)v(s)ds$$

with $\gamma(s)v(s) = \beta v s^{-1/2}/2$. However, the physical description of this form of the friction coefficient is not clear. We also note that Eq. 3 is applicable to the case of a worm-like polyelectrolyte in a constant electric field (*E*). As discussed by J. M. Schurr and S. B. Smith [*Biopolymers* **29**, 1161 (1990)], the tension in a chain with effective linear charge density ρ is given by $F(s) = \rho E s$. This relation is analogous to the form $F(s) = \gamma v s$ for a free-draining chain in a constant flow.
16. B. H. Zimm and S. D. Levene, *Q. Rev. Biophys.* **25**, 171 (1992).
17. R. G. Larson and J. J. Magda, *Macromolecules* **22**, 3004 (1989).
18. This result is consistent with the estimate of the drag force in the experiment of Smith *et al.* (*4*): In calculating the hydrodynamic force applied to the end of the chain, they increased the radius of the 2.9-μm-diameter microsphere by 0.7 μm to account for the hydrodynamic drag of their 32.6-μm-long DNA.
19. W. Kuhn, *Kolloid-Z.* **68**, 2 (1934); R. B. Bird, *Dynamics of Polymeric Liquids* (Wiley, New York, 1987) vol. 2, pp. 19–20 and 55–109.
20. Besides the contribution to the relaxation from higher- order modes, the chain may not have sufficient time to fully "explore" its phase space, and consequently, its elasticity may be different from the steady-state values.
21. F. Brochard-Wyart, *Europhys. Lett.* **23**, 105 (1993). The dynamics of the unwinding process was also analyzed within the blob model by F. Brochard-Wyart, H. Hervet, and P. Pincus [*ibid.* **23**, 511 (1994)], and there is a recent preprint (F. Brochard-Wyart) on the stretching of polymers in strong flows.
22. B. H. Zimm, personal communication.
23. J. G. Kirkwood, *J. Polym. Sci.* **12**, 1 (1953); _____ and J. Riseman, *J. Chem. Phys.* **16**, 565 (1948); *ibid.* **22**, 1626 (1954).
24. R. G. Larson, T. T. Perkins, D. E. Smith, S. Chu, in preparation.
25. J. T. Finer, R. M. Simmons, J. A. Spudich, *Nature* **368**, 113 (1994); R. M. Simmons, J. T. Finer, S. Chu, J. A. Spudich, in preparation.
26. The cover slip and microscope slide were separated by two 75-μm wires and sealed with epoxy. We created the optical tweezers by focusing a 175-mW Nd:yttrium-aluminum-garnet laser beam with an oil-immersed microscope objective (Zeiss ×63; numerical aperture, 1.4). The DNA was stained with 0.1 μM TOTO-1 (Molecular Probes), excited by 488-nm light from an Ar-ion laser and imaged with an intensified video camera (Hamamatsu C2400-08). The molecules were observed in an aqueous solution of 10 mM tris-HCl (pH 8), 1 mM EDTA, 2 mM NaCl, 0.8% β-mercaptoethanol, glucose oxidase (50 μg/ml), 0.1% glucose, and catalase (10 μg/ml). We constructed DNA molecules up to about 100 μm long by ligating together several λ-phage DNAs (16.3 μm) and linking them to a 0.3-μm or 1-μm latex sphere by a streptavidin-biotin bond as in (*5*). At this dye concentration, we measured the length of a single λ-DNA to be 22 μm by attaching each end to a 1-μm microsphere and stretching it between two optical traps with a peak force of order 10 pN. Variation of lengths from multiples of 22 μm were probably due to shearing of the DNA attached to a microsphere during pipetting.
27. The motor was stable to within 1% as determined by a signal analysis of the pulses from its 0.1 μm per pulse optical encoder. A Fourier transform of 400 extension measurements exhibited no peaks in the spectrum, showing that the fluctuations were not driven by mechanical resonances.

28. We measured the extensions by allowing the chain to reach its equilibrium extension and then digitizing 40 video frames with a delay (0.3 to 1.2 s) between each frame to allow the fluctuating chain to "explore" completely the phase space of accessible conformations. We measured the extension of the molecule along the direction of flow using a computer-generated cursor, and the average extension (x) and its standard deviation σ_x were calculated at each velocity from the 40 individual extension measurements.

29. This work was supported in part by grants from the U.S. Air Force Office of Scientific Research, the National Science Foundation, and the Human Frontier Science Program, and by an endowment established by Theodore and Frances Geballe. We acknowledge the generous assistance of J. Spudich, J. Finer, G. Nuckolls, and H. Goodson, including support through NIH grant 33289 to J. Spudich. We acknowledge helpful discussions with and a theoretical model provided by B. Zimm. We are grateful for the elasticity data provided by S. Smith. We also acknowledge helpful discussions with J. Marko, S. R. Quake, and J. L. Viovy. The work of T.T.P. was supported in part, under Office of Naval Research contract N00014-91-C-0170 through the Stanford Picosecond Free Electron Laser Center.

18 October 1994; accepted 2 February 1995

Muscle Efficiency and Elastic Storage in the Flight Motor of *Drosophila*

Michael H. Dickinson* and John R. B. Lighton

Insects could minimize the high energetic costs of flight in two ways: by employing high-efficiency muscles and by using elastic elements within the thorax to recover energy expended accelerating the wings. However, because muscle efficiency and elastic storage have proven difficult variables to measure, it is not known which of these strategies is actually used. By comparison of mechanical power measurements based on gas exchange with simultaneously measured flight kinematics in *Drosophila*, a method was developed for determining both the mechanical efficiency and the minimum degree of elastic storage within the flight motor. Muscle efficiency values of 10 percent suggest that insects may minimize energy use in flight by employing an elastic flight motor rather than by using extraordinarily efficient muscles. Further, because of the trade-off between inertial and aerodynamic power throughout the wing stroke, an elastic storage capacity as low as 10 percent may be enough to minimize the energetic costs of flight.

Flight is an energetically costly form of locomotion, requiring metabolic rates as high as 100 times the resting rate (*1*). Most of the total energy required for flight is dissipated as heat in the flight musculature. For hovering animals, the remaining mechanical energy is divided into three components: induced power required to generate lift, profile power necessary to overcome drag on the wings, and inertial power required to accelerate and decelerate the wings during stroke reversal (*2*). Previous comparisons of total metabolic rate and estimated power output suggest that insects minimize the high cost of flight either by using highly efficient muscles or by recovering inertial power through elastic storage (*3*). It is not certain, however, which of these two strategies is actually used.

Female *Drosophila hydei* were tethered and flown in a flight arena that measured the frequency and amplitude of the wing stroke as well as the yaw torque produced by the animal (Fig. 1). The fly and the torque transducer were enclosed in a respirometry chamber and surrounded by a visual panorama consisting of a dark stripe on a bright background. All experiments were done under closed-loop conditions such that the yaw torque produced by the fly was used to control the angular velocity of the stripe. Under these conditions, tethered flies actively modulated yaw torque through changes in wingbeat kinematics in order to fix the position of the stripe in the front portion of their visual field (*4*). In order to increase the variations in wingbeat amplitude and stroke amplitude, sinusoid and square wave voltage biases were added to the control signal in some experiments. Under these conditions, flies actively stabilized the stripe position by modulating flight kinematics in order to generate a compensatory torque opposite to the imposed bias. Additional modulation of wingbeat kinematics in some experiments was achieved by modulating the gain of the closed-loop feedback. These active modulations in wing stroke amplitude and frequency produced by these manipulations provided a useful and rigorous means for comparing respirometric and kinematic estimates of mechanical power.

A representative flight sequence is displayed in Fig. 2 and shows the simultaneous measurements of metabolic cost, stroke amplitude (summed from the two wings), wingbeat frequency, and yaw torque during the application of a sinusoidal bias under closed-loop conditions. As in all experiments, the fly was capable of stabilizing the visual stripe by generating a sinusoidal yaw torque to compensate for the applied bias. During this modulation in torque, the metabolic cost oscillates at roughly twice the bias frequency and is highly correlated with changes in wingbeat frequency and stroke amplitude.

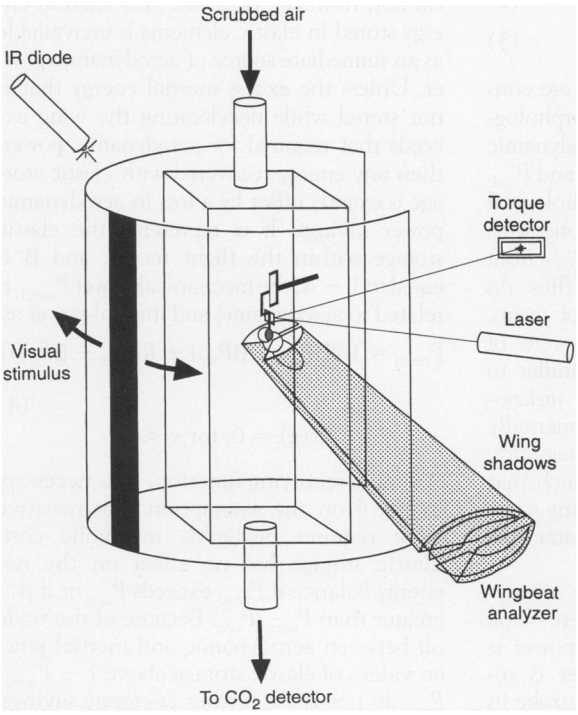

Fig. 1. Experimental apparatus for simultaneously measuring metabolic output and wingbeat kinematics of *Drosophila* during tethered flight. Flies were tethered with light-activated adhesive to a yaw torque transducer that optically tracks the angular deflection of a laser beam aimed at a small mirror mounted to the fly's tether. The fly was enclosed within a 30-ml rectangular acrylic and glass respirometry chamber. Room air was scrubbed of water and CO_2, pulled through the flight chamber at a rate of 150 ml min^{-1}, and sampled by a CO_2 analyzer (*11*). The wingbeat frequency and wing stroke amplitude of the flies were measured continuously by optical tracking of the shadows of the two wings cast by an infrared light source (*12*). The respirometry chamber was enclosed in a close-packed cylindrical array of 720 green light-emitting diodes that produced a 30° dark stripe on a bright background.

M. H. Dickinson, Department of Organismal Biology and Anatomy, University of Chicago, Chicago, IL 60637, USA.
J. R. B. Lighton, Department of Biology, University of Utah, Salt Lake City, UT 84112, USA.
*To whom correspondence should be addressed.